RX AND Z-MODE GROWTH RATES AND PROPAGATION AT CAVITY BOUNDARIES

R. L. Mutel*, I. W. Christopher*, J. D. Menietti*, D. A. Gurnett*, J. S. Pickett*, A. Masson†, A. Fazakerley‡, and E. Lucek§

Abstract

Recent Cluster WBD observations in the Earth's auroral acceleration region have detected trapped Z mode auroral kilometric radiation while the spacecraft were entering a deep density cavity. The Z mode has a clear cutoff at the local upper hybrid resonance frequency, while RX mode radiation is detected above the RX mode cutoff frequency. The small gap between the upper hybrid resonance and the RX mode cutoff frequencies is proportional to the local electron density as expected from cold plasma theory. The width of the observed gap provides a new sensitive measure of the ambient electron density. In addition, the relative intensities of RX and Z mode radiation provide a sensitive probe of the plasma $\beta = \omega_{pe}/\Omega_{ce}$ at the source since the growth rates, although identical in form, have different ranges of allowed resonant radii which depend on β. In particular, the RX mode growth is favored for low β, while the Z mode is favored at higher β. The observed mode intensities and β's appear to be consistent with this model, and favor generation of Z mode at the source over models in which Z mode is generated by mode-conversion at cavity boundaries. These are the first multi-point direct measurements of mode-specific AKR propagation in the auroral acceleration region of any planet.

1 Introduction

Auroral kilometric radiation is generated by the cyclotron maser instability (CMI), driven by mildly relativistic electron beams in the Earth's auroral regions (e.g., Treumann [2006] and references therein). The electron beams are downward-going at high altitudes, but acquire increasing perpendicular energy as they encounter the Earth's converging magnetic field. This results in an unstable velocity distribution ($\partial f/\partial v_\perp > 0$) which drives

* *Department of Physics and Astronomy, University of Iowa, Iowa City, IA 52242, USA*
† *ESA/ESTEC, 2200 AG Noordwijk, Netherlands*
‡ *Mullard Space Science Lab., University College London, London RH5 6NT, UK*
§ *Imperial College London, Prince Consort Road, London, SW7 2BW, UK*

the maser instability. The source regions reside in auroral cavities in which the electron plasma frequency is much less than the cyclotron frequency (i.e., $\omega_{pe} \ll \Omega_{ce}$, Calvert 1981; Delory et al. 1998). Low densities favor wave growth in the extraordinary mode, although ordinary mode is also detected, albeit at much lower intensities [Benson et al., 1988; Hanasz et al., 2003].

The extraordinary mode has two branches depending on the emission frequency. For waves below the upper hybrid resonance frequency, the emission is Z mode, while waves above the RX cutoff frequency are in the RX mode[1]. The Z branch emission is trapped i.e., it cannot escape to free space, since the upper hybrid resonance level always lies between the source and free space. Consequently, most observations of AKR have been of RX mode emission. Only spacecraft located in the auroral acceleration region below the UHR resonance level can detect Z mode emission.

In this paper, we report on the first simultaneous observations of RX and Z mode emission detected by multiple spacecraft while they were traversing the Earth's auroral acceleration region. From the narrow frequency gaps separating these modes, we derive ambient electron densities and compare them with density measurements derived from observation of low-frequency hiss emission. We also compare CMI growth rates for RX and Z modes, and deduce properties of the source region from the observed intensity ratios. Finally, we discuss propagation of RX and Z modes through the density wall surrounding the nearby auroral cavities in which the AKR sources are located, and compare with numerical models.

2 Wave Modes in a Cold Magnetized Plasma

We first briefly review aspects of wave propagation in a cold magnetized plasma that will be useful for analyzing RX/Z mode observations. As shown in Figure 1, there are four possible wave modes in cold magnetized plasmas viz. W (a.k.a. whistler), LO, Z, and RX [Gurnett and Bhattacharjee, 2005]. While all four modes have low-frequency cutoffs, the W and Z modes also have upper frequency resonances where the waves become electrostatic.

The LO and RX modes can propagate to free-space, where in the limit $\omega \gg (\omega_{pe}, \Omega_{ce})$ they are purely transverse, oppositely circularly polarized waves. The notations LO and RX derive from the helicity of each mode when propagating parallel to the magnetic field: LO is left-circularly polarized while RX is right-circularly polarized. However, for the general case of oblique propagation, both modes are elliptically polarized and are not purely transverse.

Z mode waves can propagate from the lower 'L=0' cutoff frequency to the upper hybrid resonance (UHR) frequency, where they become electrostatic. The UHR frequency for

[1] Note that the term 'mode' is commonly used to describe ordinary and extraordinary wave modes as well as the branches within each mode (LO, W for ordinary; RX, Z for extraordinary. Although somewhat confusing, we will continue this practice.

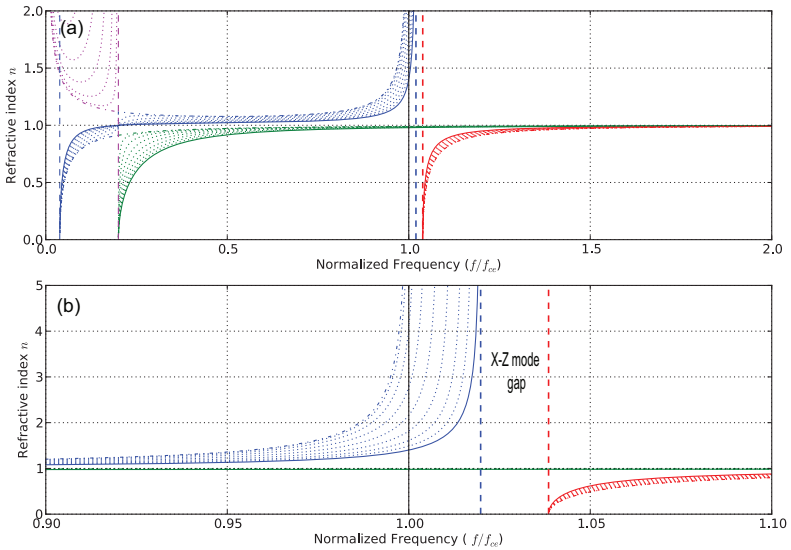

Figure 1: Refractive index vs normalized frequency (ω/ω_{ce}) for the four propagating waves in a cold magnetized plasma for the case $\omega_{pe} = 0.2\ \Omega_{ce}$. Modes are coded by color: W mode (magenta), Z mode (blue), LO mode (green), and RX mode (red). Angle of propagation varies from parallel (dot-dash line) to perpendicular (solid line). (b) Magnified view in the normalized frequency range 0.90 —1.10. Note the gap between the Z mode upper hybrid resonance and the RX mode cutoff frequencies.

waves propagating perpendicular to the local magnetic field can be written

$$\omega_{uhr} = \left(\Omega_{ce}^2 + \omega_{pe}^2\right)^{\frac{1}{2}} = \Omega_{ce}\left(1+\beta^2\right)^{\frac{1}{2}} \approx \Omega_{ce}\left(1+\frac{1}{2}\beta^2\right) \ , \tag{1}$$

where we assume $\beta \equiv \omega_{pe}/\Omega_{ce} \ll 1$. On the other hand, RX mode waves have a low frequency cutoff given by

$$\omega_{rx} = \frac{\Omega_{ce}}{2} + \left[\left(\frac{\Omega_{ce}}{2}\right)^2 + \omega_{pe}^2\right]^{\frac{1}{2}} \approx \Omega_{ce}\left(1+\beta^2\right) \ . \tag{2}$$

Comparing these equations, we see that $\omega_{rx} > \omega_{uhr}$ for all $\beta > 0$, so there is a frequency gap between these modes in which neither mode can propagate. The gap width is proportional to the ambient electron density and inversely proportional to the magnetic field strength,

$$\Delta\omega = \omega_{rx} - \omega_{uhr} \approx \frac{1}{2}\Omega_{ce}\beta^2 = 15\ kHz\left(\frac{n_e}{B}\right) \tag{3}$$

where B is the magnetic field (nT) and n_e is the electron density (cm^{-3}).

3 Cluster Observations of RX and Z Mode Waves in the Earth's Auroral Acceleration Region

The Cluster mission consists of a tetrahedral constellation of four identical spacecraft in a highly elliptical geocentric orbit [Escoubet et al., 2001]. Each spacecraft is equipped with eleven instruments measuring a wide range of ambient plasma and field characteristics. This paper utilizes data from three of these instruments. The Cluster wideband data (WBD) receiver records electric field waveforms between 25 Hz and 577 kHz from one of two dipole antennas oriented orthogonal to the spacecraft spin axis [Gurnett et al., 2001]. The resonance sounder and wave analyzer (WHISPER) measures the total electron density using both passive and active sounding [Dècrèau et al. 2001; Trotignon et al., 2003]. The flux gate magnetometer (FGM) measures the magnetic field using triaxial flux gate magnetometers [Balogh et al., 1997].

The constellation's original orbit was unsuitable for studying in situ auroral processes since perigee was $4.0R_e$ at low magnetic latitude. However, the orbit has gradually evolved so that by May 2009 the spacecraft traversed the Earth's northern auroral acceleration region for the first time. This was followed by a second series of encounters between December 2009 and February 2010. During these encounters, several WBD spectrum show clear evidence for simultaneous Z and RX mode emission, with a small gap corresponding to the expected frequency difference between the UHR resonance and the RX mode cutoff frequency as described above. In this paper, we analyze an event from the second encounter when some of the spacecraft flew through an active auroral cavity. These multi-spacecraft observations allow us to estimate relative growth rates and propagation characteristics of Z and RX mode radiation as it emerges from the auroral cavity.

3.1 The 12 Dec 2009 Encounter

Figure 2a shows a 3-dimensional view of Cluster spacecraft trajectories during an auroral region pass on 12 Dec 2009. C3 and C4 have almost identical trajectories, but C3 lags C4 by 182 sec. C1 is on the nearly same magnetic line as C3 but is displaced about 1,500 km higher. C2's trajectory is at a similar altitude as C3 and C4, but is 1000 - 2000 km north of the other spacecraft's trajectories. Figure 2b is a 'top-down' view superposed on a geomagnetic coordinate grid. The C1-C3-C4 trajectories are nearly tangential to the auroral oval at magnetic latitude +72° between 04:30 and 04:45 UT. Figure 2c shows the electron density measured on C1, C3, and C4 derived from WHISPER data. The shaded region between 04:26 — 04:34 UT corresponds to the WBD spectra shown in Figure 3.

The density profiles indicate that the spacecraft entered a density-depleted region (cavity) at approximately 04:30 UT. Note that the density profiles for C3 and C4 are very similar but offset by 182 sec, consistent with time lag between C3 and C4 as described above. This indicates that the density cavity structure was nearly constant over this time period.

An overview of WBD spectra for all four spacecraft during this encounter is shown in Figure 3. We interpret the frequency gap evident in the C3 and C4 (and possibly C2) spectra as resulting from the X-Z mode gap described by equation 3. In Figure 4 we display the C4 spectrum in more detail, showing the interval 04:25 — 04:30 UT. The top

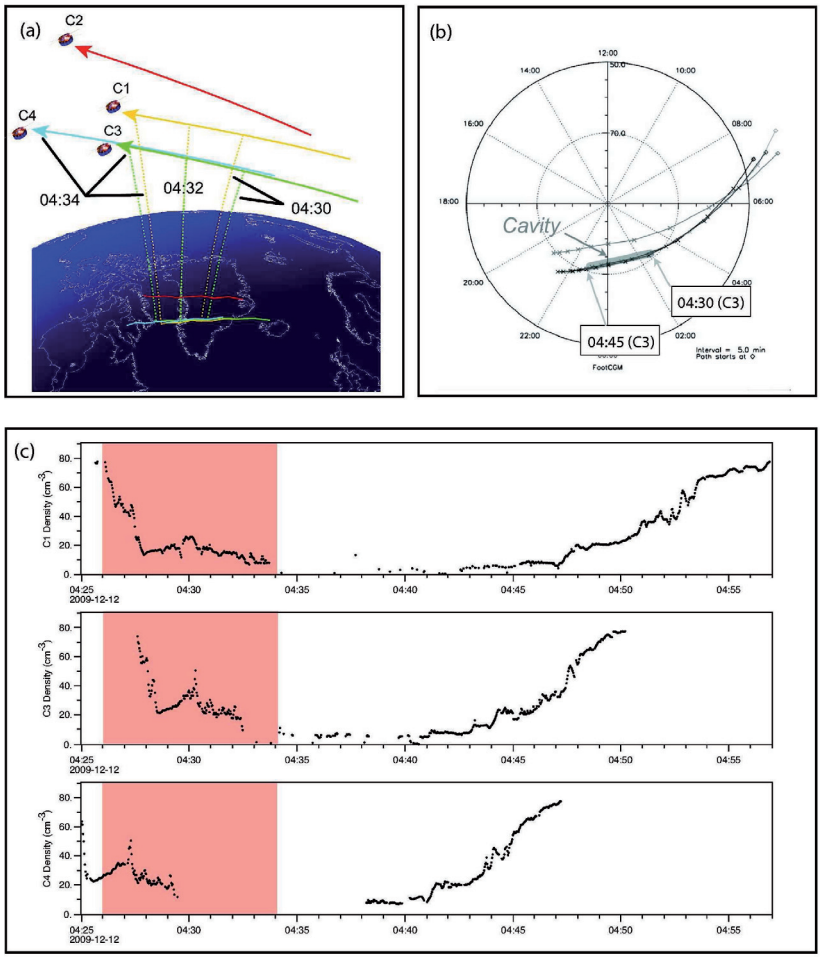

Figure 2: (a) Trajectories of Cluster spacecraft C1— C4 on 12 Dec 2009 from 04:10 to 05:00 UT. Note that the trajectory of C3 is very close to C4 but trails by 182 sec. (b) Spacecraft trajectories projected onto a geomagnetic coordinate grid. (c) Electron density measurements for C1, C3, and C4 derived from WHISPER data. The pink shaded regions delineate the time interval 04:26 — 04:34 UT corresponding to the WBD spectra shown in Figure 3.

and middle panels display the spectrum, the latter overlaid by white lines showing the local electron cyclotron frequency (dashed line) and the computed upper hybrid resonance frequency (dotted line). The observed electron density from WHISPER is shown in the lower panel.

The upper panel in Figure 5 shows a fit to the gap in the interval 04:26:05 — 04:27:56

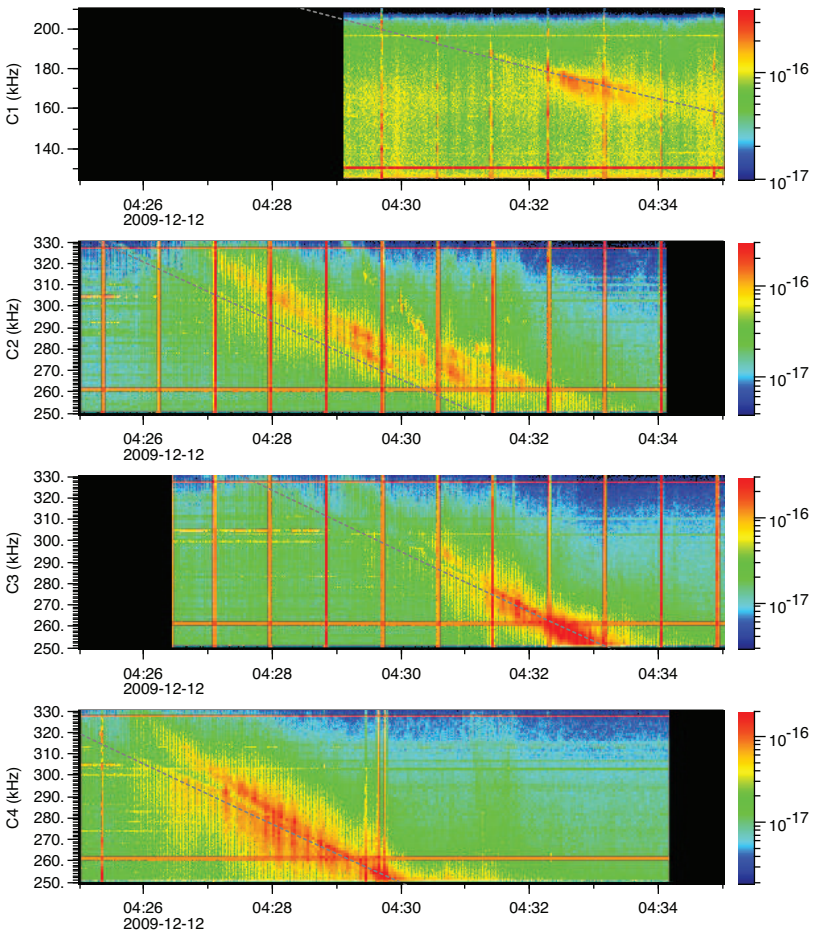

Figure 3: Overview of Cluster WBD dynamic spectra observed at spacecraft C1 — C4 on 12 Dec 2009 from 04:25 to 04:34 UT. The X-Z mode gap is evident in C3 and C4 spectra, which are very similar but offset by 182 sec. This is consistent with the C3-C4 trajectory lag and the nearly constant density structure seen in Figure 2. The dashed lines mark the local electron cyclotron frequency at each spacecraft determined from FGM magnetometer measurements.

UT. The green line is the local electron cyclotron frequency, while the red and blue lines are the upper hybrid and RX cutoff frequencies respectively, computed using the measured density and magnetic field. The black squares and crosses are the hand-fitted edges of the observed gap. The lower panel shows the electron density measured using

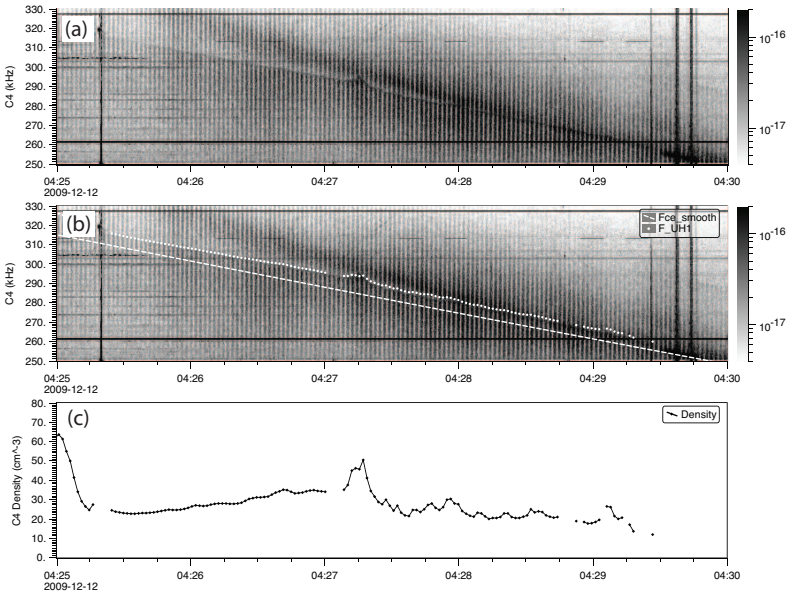

Figure 4: (a) Cluster spacecraft C4 WBD dynamic spectrum on 12 Dec 2009 from 04:25 to 04:30 UT. Note the sloping gap resulting from the small frequency separation between the Z mode upper hybrid resonance and the RX mode cutoff frequencies. (b) Same as (a), but with electron cyclotron frequency (dashed line) and upper hybrid resonance frequency (dotted line) calculated from measured electron density superposed. (c) Electron density measured using WHISPER passive-mode observations of auroral hiss cutoffs.

WHISPER instrument (black line) compared with derived density from observed gap (green points) using equation 3. We have applied a +1% scale factor increase to the FGM-derived magnetic field measurements to allow consistency with the UHR frequency profile. This is also consistent with the FGM uncertainty in absolute field values inferred from comparisons between FGM and IGRF field values [Woodfield et al., 2006].

Although there is good agreement between measured and gap-derived electron density in the mean, there are significant differences on short timescales. This results primarily from the mediocre RX mode fit: There is very good agreement between the computed and observed upper hybrid frequencies, while the computed RX mode cutoff frequency does not agree as well, resulting in the density discrepancies. This may be partially a result of a less well-defined RX mode cutoff boundary than the upper hybrid resonance, but may also result from a warm plasma correction to the RX mode cutoff frequency (e.g., Winglee [1985a]).

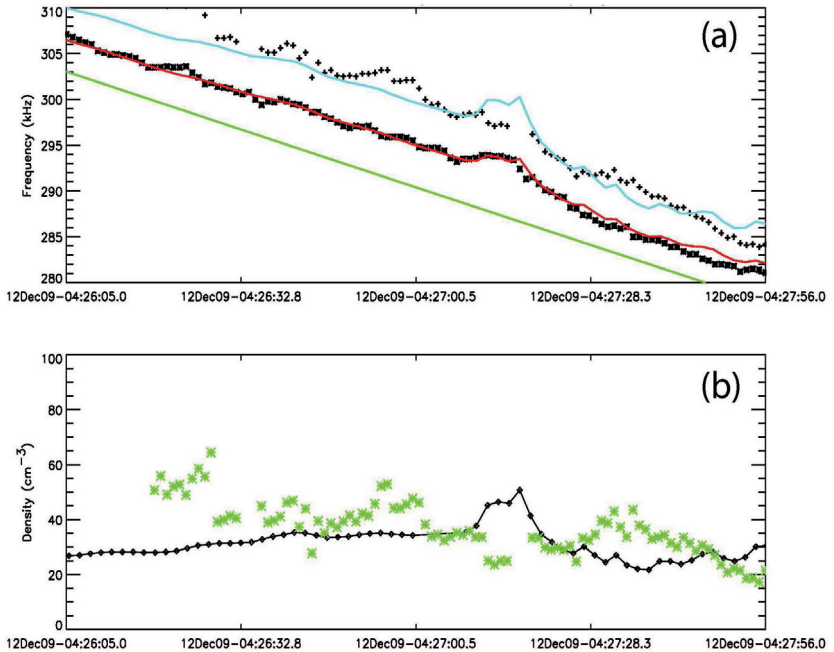

Figure 5: (a) Fit to RX-Z mode gap in C4 WBD spectrum on 12 Dec 2009 from 04:26:05 — 04:27:56 UT (cf. Figure 4). The green line is the local electron cyclotron frequency computed from FGM magnetic field measurements. The red and blue lines are the upper hybrid and RX cutoff frequencies respectively, computed using the measured density and magnetic field. The black squares and crosses are estimated edges of the observed gap. (b) Electron density measured using WHISPER instrument (black line) compared with derived density from observed gap (green points) using equation 3.

3.2 Propagation of RX, Z Mode

Z mode radiation is bound from below by a surface defined by the lower 'L=0' cutoff frequency and from above by a surface defined by the UHR frequency. RX mode radiation is bound only from below by the RX cutoff surface. Since AKR emission originates in low-density cavities and propagates to regions with higher density, these surfaces change topology as the density changes. This is illustrated in Figure. 6 which shows accessible regions for X and Z rays originating at a source (marked with a star) located in a vertical density cavity with B-field pointing up. The lower shaded region (labeled Z-mode) is accessible to Z mode rays originating at the source, while the upper shaded region (labeled X mode) is accessible to X mode rays. In the region between these surfaces neither Z nor RX mode can propagate.

A spacecraft moving on a trajectory indicated by the black arrow will detect Z mode

radiation at a given frequency until it traverses the gap, after which it will detect RX mode. The inset reproduces part of the observed WBD spectrum on 12 Dec 2009, in agreement with the described geometry.

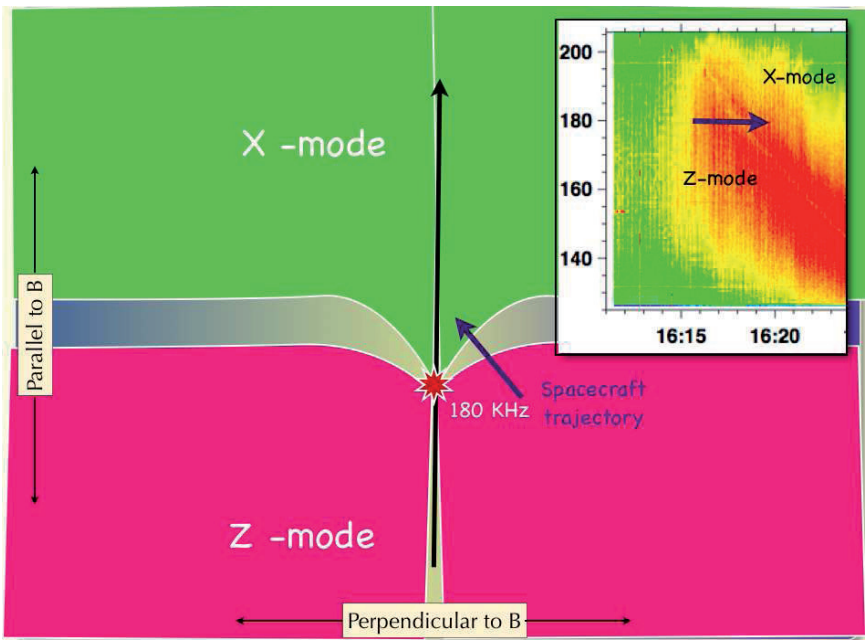

Figure 6: Cartoon illustrating allowed propagation regions for X and Z-mode radiation emanating from a vertical cavity with higher density walls. The source region is located at a fixed point ($f_{ce} = 180$ KHz) in the cavity, while the cavity is aligned with the ambient magnetic field (vertical black arrow). A spacecraft whose trajectory is approaching an auroral cavity (blue arrow) will detect Z-mode radiation, followed by a gap, then X-mode radiation. This is seen on observed spectra (inset).

3.3 Density Dependence of CMI Growth Rates

The temporal growth rate of the cyclotron maser for extraordinary mode waves can be written [Mutel et al., 2010]

$$\frac{\omega_i}{\Omega} = \frac{\pi^2}{4}\frac{n_h}{n_e}\beta^2 v_r^2 \int_0^\pi d\varphi \, \sin^2\varphi \left[\frac{\partial f}{\partial v_\perp} + \frac{k_\parallel v_\perp}{\Omega}\frac{\partial f}{\partial v_\parallel}\right]_{|\vec{v}|=v_r} \tag{4}$$

where velocities are normalized to c, f is the normalized velocity distribution function, n_h/n_e the ratio of hot to total electron density, β the ratio of electron plasma to cyclotron

frequencies, and the integration is along a semi-circle of constant radius v_r in the $(v_\parallel, v_\perp)$ plane. The resonant velocity v_r is given by

$$v_r = \left[(k_\parallel c/\Omega)^2 - 2\delta\omega\right]^{\frac{1}{2}} \approx (-2\delta\omega)^{\frac{1}{2}} \tag{5}$$

where Ω is the cyclotron frequency, the fractional frequency is $\delta\omega = (\omega - \Omega)/\Omega$, and the approximate expression is valid for $k_\parallel \ll k$ as is observed in AKR source regions by FAST (e.g., Delory et al. [1998]).

Equation 4 applies equally to the RX and Z modes, since they are both extraordinary modes. However, growth rates depend on whether the resonant radius for each mode samples an unstable region in phase space (i.e., where $\partial f/\partial v_\perp > 0$). Since the resonant radius depends on fractional frequency, the allowed range of v_r depends in turn on mode. For RX mode, the allowed frequency range is $\omega_{rx}/\Omega < 1 + \delta\omega < 1$ whereas for Z mode the allowed range is $\omega_L/\Omega < 1 + \delta\omega < \omega_{uhr}/\Omega$. The corresponding allowed velocity ranges are

$$0 < v_r < \sqrt{2(1 - \omega_{rx}/\Omega)}\ ,$$

for RX mode, and

$$\sqrt{2(1 - \omega_{uhr}/\Omega)} < v_r < \sqrt{2(1 - \omega_L/\Omega)}$$

for Z mode.

Since both ω_{uhr} and ω_{rx} depend on density, the above velocity ranges will also depend on density, with RX mode favored at low densities, Z mode at higher densities.

Figure 7 shows CMI growth rates calculated using a DGH ring model distribution [Dory et al., 1965] with a mean energy 10 keV and plasma β= 0.03, 0.075, and 0.13. The color shading indicates the allowed range of v_r for RX mode (blue) and Z mode (pink). Low β plasma favors RX mode, while high β plasma favors Z mode (cf. Winglee 1985b, Dusenberry et al. 1985). Inspection of Figure 3 shows that C3 and C4 spectra have comparable RX and Z mode intensities, indicating an intermediate value of β, while C1's spectrum appears to be dominated by Z mode, indicating a higher β. This is consistent with β computed from measured fields and densities: For C1 at 04:32 UT, β = 0.19, whereas for C3 β = 0.13. We also note that given the comparable intensities of RX and Z mode radiation, and compatibility with expected CMI growth rates at the measured intermediate β's, it appears likely that Z mode is generated at the CMI source rather than generated by mode-conversion at the cavity boundary, as suggested by some numerical models (e.g. Pritchett et al. [2002]).

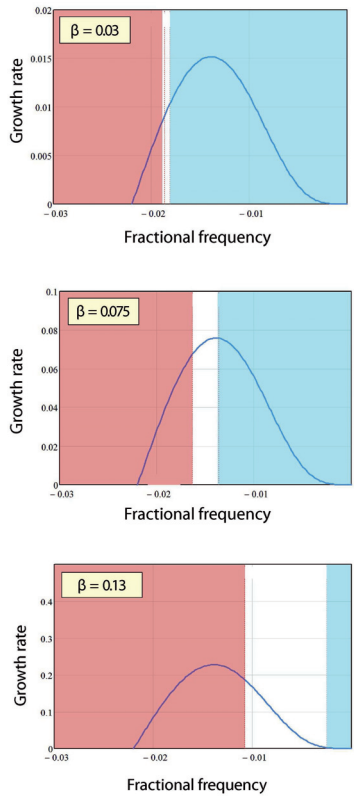

Figure 7: CMI growth rates versus fractional frequency for DGH velocity distribution model with mean ring energy $\bar{E} = 10$ keV and plasma $\beta = 0.03$ (top panel), 0.075 (middle panel), and 0.13 (lower panel). The allowed frequencies for Z-mode and X-mode are shown in red and blue respectively. Note the dominance of X-mode and low density, comparable X/Z mode growth at intermediate density, and Z-mode dominance at high density.

References

Balogh, A., M. W. Dunlop, S. W. H. Cowley, D. J. Southwood, J. G. Thomlinson, K. H. Glassmeier, G. Musmann, H. Luhr, S. Buchert, M. H. Acuna, D. H. Fairfield, J. A. Slavin, W. Riedler, K. Schwingenschuh, and M. G. Kivelson, The Cluster Magnetic Field Investigation, *Space Sci. Rev.*, **79**, 65-91, 1997.

Benson, R., M. Mellott, R. Huff, and D. Gurnett, Ordinary mode auroral kilometric radiation fine structure observed by DE–1, *J. Geophys. Res.*, **93**, 7515, 1988.

Calvert, W., The auroral plasma cavity, *Geophys. Res. Lett.*, **8**, 919-921, 1981.

Dècrèau, P. M. E., P. Fergeau, V. Krannosels'kikh, M. Leveque, Ph. Martin, O. Randri-

amboarison, F. X. Sene, J. G. Trotignon, P. Canu, and P. B. Mogensen, Whisper, a Resonance Sounder and Wave Analyser: Performances and Perspectives for the Cluster Mission, *Space Sci. Rev.*, **79**, 157-193, 1997.

Delory, G. T., R. E. Ergun, C. W. Carlson, L. Muschietti, C. C. Chaston, W. Peria, J. P. McFadden, and R. Strangeway, FAST observations of electron distributions within AKR source regions, *Geophys. Res. Lett.*, **25**, 2069, 1998.

Dory, R., G. Guest, and E. Harris, Unstable electrostatic plasma waves propagating perpendicular to a magnetic field, *Physical Review Letters*, **14**, 131-133, 1965.

Dusenbery, P. B., and L. R. Lyons, Generation of Z Mode Radiation by Diffuse Auroral Electron Precipitation, *J. Geophys. Res.*, **90**, 2915, 1985.

Escoubet, P., M. Fehringer, and M. Goldstein, Introduction to the Cluster Mission, *Ann. Geophys.*, **19**, 1197-1200, 2001.

Gurnett, D. A. and A. Bhattacharjee, Introduction to Plasma Physics, Cambridge Univ. Press, 2005.

Gurnett, D. A., R. L. Huff, J. S. Pickett, A. M. Persoon, R. L. Mutel, I. W. Christopher, C. A. Kletzing, U. S. Inan, W. L. Martin, J.–L. Bougeret, H. St. C. Alleyne, and K. H. Yearby, First results from the Cluster wideband plasma wave investigation, *Ann. Geophys.*, **19**, 1259-1272, 2001.

Hanasz, J., M. Panchenko, H. de Feraudy, R. Schreiber, and M. M. Mogilevsky, Occurrence distributions of the auroral kilometric radiation ordinary and extraordinary wave modes *J. Geophys. Res.*, **108**, doi:10.1029/2002JA009579, 2003.

Mutel, R. L., J. D. Menietti, D. A. Gurnett, W. Kurth, P. Schippers, C. Lynch, L. Lamy, C. Arridge, and B. Cecconi, CMI growth rates for Saturnian kilometric radiation, *Geophys. Res. Lett.*, **37**, L19105, doi:10.1029/ 2010GL044940, 2010.

Pritchett, P. L., R. J. Strangeway, R. E. Ergun, and C. W. Carlson, Generation and propagation of cyclotron maser emissions in the finite auroral kilometric radiation source cavity, *J. Geophys. Res.*, **107**, doi:10.1029/2002JA009403, 2002.

Treumann, R. A., The electron–cyclotron maser for astrophysical application, *Astron. Astrophys. Rev.*, **13**, 229–315, 2006.

Trotignon, J. G., P. M. E. Dècrèau, J. L. Rauch, E. Le Guirriec, P. Canu, and F. Darrouzet, The Whisper Relaxation Sounder Onboard Cluster: A Powerful Tool for Space Plasma Diagnosis around the Earth, *Cosm. Res.*, **41**, 345–348, 2003.

Winglee, R., Effects of a finite plasma temperature on electron-cyclotron maser emission, *Astrophys. J.*, **291**, 160-169, 1985a.

Winglee, R. M., Fundamental and harmonic electron cyclotron maser emission, *J. Geophys. Res.*, **90**, 9663, 1985b.

Woodfield, E., M. Dunlap, R. Holme, J. Davies, and M. Hapgood, A statistical comparison of Cluster magnetic data with the Tsyanenko 2001 model, 36th COSPAR Scientific Assembly, 36, 2386, 2006.